Monthly Notices of the ROYAL ASTRONOMICAL SOCIETY

MNRAS **550**, 1–8 (2026) https://doi.org/10.1093/mnras/stag1077
Advance Access publication 2026 June 08

# *JWST* spectroscopy of SN 2010da/NGC 300 ULX-1: a surviving star hidden by dust

Emma R. Beasor,[1★] Ryan Lau,[2] Nathan Smith,[3] Dominic J. Walton,[4] Marianne Heida[5] and Ben Davies[6]

[1]*Astrophysics Research Institute, Liverpool John Moores University, IC2, 146 Brownlow Hill, Liverpool L3 5RF, UK*
[2]*IPAC, California Institute of Technology, 1200 E. California Blvd, Pasadena, CA 91125, USA*
[3]*Steward Observatory, University of Arizona, 933 North Cherry Avenue, Tucson, AZ 85721-0065, USA*
[4]*Centre for Astrophysics Research, University of Hertfordshire, College Lane, Hatfield AL10 9AB, UK*
[5]*National Institute for Public Health and the Environment (RIVM), P.O. Box 1, NL-3720 BA, Bilthoven, the Netherlands*
[6]*Independent researcher*

Accepted 2026 June 1. Received 2026 June 1; in original form 2026 February 9

## ABSTRACT

We present new James Webb Space Telescope (*JWST*) NIRSpec and MIRI integral-field spectroscopy of the remarkable system SN 2010da/NGC 300 ULX-1, the only known ultraluminous X-ray source powered by a neutron star with a supergiant donor. Our new data, taken in 2024 November, reveal that the optical and near-infrared counterpart has dramatically faded since 2018 and no longer exhibits molecular absorption features characteristic of a red supergiant. Instead, the spectral energy distribution (SED) shows the donor has returned to its pre-outburst appearance, and is dominated by infrared continuum consistent with an optically thick warm (≈900 K) dust shell. The bolometric luminosity indicates the presence of a surviving luminous source with $\log(L/\mathrm{L}_\odot) = 4.11 \pm 0.02$. Radiative transfer modelling of the mid-infrared SED reveals a broad emission feature peaking near ∼11 μm, best reproduced by silicon carbide (SiC) dust grains, a composition typically associated with carbon-rich evolved stars. We rule out a failed supernova scenario, which would predict a large drop in luminosity and continued fading. Given the association of SiC dust with asymptotic giant branch (AGB) stars, we suggest the donor star may be an AGB star that has survived and is now heavily enshrouded – having returned to a dust-obscured state following a transient post-outburst phase in which the system appeared as a red supergiant. We propose a revised evolutionary timeline in which the 2010 outburst initiated sustained super-Eddington accretion and temporarily altered the circumstellar environment. These observations provide rare insight into eruptive mass-loss, dust formation, and binary interaction in a unique system.

**Key words:** supergiants – stars: neutron – X-rays: binaries – transients: supernovae.

## 1 INTRODUCTION

Stellar evolution underpins all areas of astrophysics. Massive stars in particular have major influence on many fundamental galactic/extragalactic observables, since their explosive deaths enrich the universe with heavy elements and drive chemical evolution. However, modern surveys and advances in stellar modelling are highlighting significant gaps in our understanding. While canonical theory suggests stars between 8–30 $\mathrm{M}_\odot$ should all die as Type II-P H-rich supernovae before leaving behind a neutron star remnant, the apparent lack of high-mass progenitors (S. Smartt 2015; B. Davies & E. R. Beasor 2020a, b) and the higher-than-expected detection rate of of binary stellar mass black holes (BHs; B. P. Abbott et al. 2017) are leading many to speculate that enhanced mass-loss phases could alter the evolutionary path and peel away the envelope of a star, forcing it to die as a H-poor Type Ibc SNe (e.g. C. Georgy 2012). However, observational estimates of wind mass-loss rates are lower (N. Smith 2014; E. R. Beasor et al. 2020) than mass-loss prescriptions used in most stellar evolution models, and observations of massive stars in galaxies and clusters show that any enhanced mass-loss phases are far too rare and short-lived to impact RSG envelopes (E. R. Beasor & N. Smith 2022). To further complicate matters, stars in this mass range are highly likely to have evolved in a binary system (H. Sana et al. 2012; M. Moe & R. Di Stefano 2017), the ultimate outcomes of which are diverse.

Some objects in the universe do undergo massive eruptions through which large amounts of mass may be ejected, most notably 'SN imposters' and luminous blue variables (LBVs) such as $\eta$ Carinae, P Cygni and SN 2009ip, among others (see N. Smith 2026 for a recent review). While the cause of these eruptions remains debated, some of them (like $\eta$ Car) are likely to be massive star merger events (N. Smith et al. 2018). These transients can reach

★ E-mail: E.R.Beasor@ljmu.ac.uk

peak magnitudes of $M_V \simeq -10$ to $-15$, but do not result in the destruction of the progenitor star (N. Smith et al. 2011a). While rare, these volatile phases may be able to significantly alter the evolutionary path of a star by removing 10s of solar masses of material in a short space of time (N. Smith et al. 2003; N. Smith & P. Hartigan 2006). As such, LBVs and SN impostors provide a unique opportunity to understand the influence of eruptive mass-loss on stellar evolution. However, the physical mechanism that powers major LBV events remains unknown.

The SN imposter SN 2010da has continued to behave in unexpected ways since its initial discovery in 2010. The event was detected in the nearby spiral galaxy NGC 300, at a distance of only 1.86 Mpc (J. J. Dalcanton et al. 2009). The visual-wavelength light curve and spectral evolution of the initial optical transient (R. Chornock & E. Berger 2010) showed similarities to LBVs and other SN impostors (N. Smith et al. 2011b). Shortly after the optical outburst, a compact, persistent X-ray source was identified at the same location, leading to speculation that the system may be a high-mass X-ray binary (HMXB) powered by accretion on to a compact object (B. Binder et al. 2011, 2016). Further X-ray observations of the system revealed luminosity above $10^{39}$ ergs s$^{-1}$ placing the system above the threshold to be classified as an ultraluminous X-ray source (ULX; see C. Pinto & D. J. Walton 2023 and M. Middleton, A. Gúrpide & D. J. Walton 2023 for recent reviews on ULXs). As such, the system was re-dubbed NGC 300 ULX-1. ULXs are the most extreme members of the X-ray binary population, and are ultimately powered by accretion from a stellar binary companion on to a compact object (see P. Kaaret, H. Feng & T. P. Roberts 2017). Furthermore, in the case of ULX-1 coherent X-ray pulsations with a period of ∼30 s were subsequently discovered (S. Carpano et al. 2018), unambiguously revealing that the accretor is a neutron star that was undergoing highly super-Eddington accretion ($L_X/L_{edd} \sim 20$) during its ULX phase.[1] This makes SN 2010da/ULX-1 the only SN impostor event known to host a NS companion, and one of the few ULX pulsars known (e.g. M. Bachetti et al. 2014; K. Y. Eksi et al. 2015; G. L. Israel et al. 2017; F. Fürst et al. 2023). The spin period of the NS showed an extreme rate of spin-up during this phase (G. Vasilopoulos et al. 2018), as expected for accretion at extreme rates. Such extreme accretion is further supported by the ∼0.25*c* outflow subsequently detected (P. Kosec et al. 2018). Broad-band X-ray data also revealed the potential presence of a cyclotron resonant scattering feature at ∼13 keV, implying a magnetic field strength of $\sim 10^{12}$ G for the NS (D. J. Walton et al. 2018), relatively typical of the field strengths seen in other NS HMXBs (see I. Caballero & J. Wilms 2012 for a review).

Other multiwavelength studies revealed additional optical, IR, and X-ray peculiarities compared to other SN impostors (R. M. Lau et al. 2016; V. A. Villar et al. 2016). These studies also revealed it to be dust enshrouded, and suggested that the source remaining after the 2010 outburst was 0.4 dex more luminous than the pre-2010 progenitor. Notably, the progenitor was suggested as a yellow supergiant consistent with an initial mass around 10–12 $M_\odot$ (V. A. Villar et al. 2016); such stars are considered to be too low in luminosity to undergo the LBV-like eruptions often invoked to explain SN impostors. Pre-outburst imaging at the location of ULX-1 reveal the progenitor was not an X-ray emitter, suggesting the 2010 outburst triggered a major shift in the system's configuration, initiating super-Eddington accretion and the ULX phase (see B. A. Binder et al. (2020) for a review of the evolution of SN 2010da/NGC 300 ULX-1).

Spectral observations of the donor star taken in 2018 showed evidence for a cool atmosphere and expanding wind (e.g. CO bandheads, TiO absorption features; see M. Heida et al. 2019). Fitting stellar atmosphere models to the spectrum showed the star resembled a red supergiant (RSG), with a temperature in the range 3650 < Teff (K) < 3900, while the *K*-band flux implies a luminosity of $\log(L/L_\odot) = 4.45 \pm 0.10$. This is distinctly different from the less luminous yellow supergiant progenitor. Fitting the full X-shooter spectrum however required two additional components; a blue excess which can be attributed to a hot blackbody where Teff = 20 000 K or a power law ($\alpha \approx 4$), likely due to reprocessed X-ray emission from the outer accretion disc, and a red excess that is likely the result of warm dust in the vicinity of the system (M. Heida et al. 2019). ULX-1 is the only X-ray pulsar system thought to contain an RSG, making the system unique. For one, there is clear potential that this system could be a progenitor for a compact object binary system (either NS–NS or NS–BH), depending on whether or not the RSG explodes as a SN or collapses directly to BH. The RSG–NS combination also places the system as a candidate Thorne–Żytkow Object (TŻO) progenitor, which is a 'star within a star' (e.g. K. S. Thorne & A. Żytkow 1975, 1977; P. Podsiadlowski, R. C. Cannon & M. J. Rees 1995; R. Hirai & P. Podsiadlowski 2022; R. Farmer et al. 2023), predicted to form when a NS is swallowed by an RSG or a red giant.

Further deepening the mystery surrounding SN2010da/NGC300 ULX-1, the source has faded significantly across X-ray, optical and infrared wavelengths since 2018 (see A.-N. Chené et al. 2025, and references within). A.-N. Chené et al. (2025) present X-ray and optical observations of SN 2010da/NGC 300 ULX–1, demonstrating that the system has exited its super-Eddington accretion phase. Continued monitoring with *Swift*/XRT shows that the super-Eddington activity has ceased, while the most recent *Chandra* detection in 2020 revealed a comparatively low X-ray luminosity of $L_X \approx 10^{37}$ erg s$^{-1}$, indicating that accretion on to the neutron star persists but is no longer supercritical. The optical detection obtained with *Gemini* in 2024 shows that the source is more than 2.5 mag fainter in the *i*-band relative to when the donor was spectroscopically identified as an RSG. Interpreting the concurrent decline in accretion rate and optical luminosity as a consequence of rapid donor-star evolution, A.-N. Chené et al. (2025) propose that the donor underwent a silent core collapse to form a BH, potentially resulting in the emergence of a nascent neutron star–BH binary system.

Here, we present new spectral data from SN2010da/NGC 300 ULX-1 taken with the ESO Very Large Telecope (*VLT*) and the *James Webb Space Telescope* (*JWST*). The paper is organized as follows. In Section 2, we discuss the observations and data from *VLT* and *JWST*. In Section 3, we present the results of our analysis, including the luminosity of ULX-1 and a comparison to the progenitor system. In Section 4, we discuss the implication of these results and a suggest a possible evolutionary scenario. Finally, in Section 5 we present our conclusions.

[1]The detection of coherent X-ray pulsations with a 30 s period unambiguously identifies the compact object as an accreting neutron star. The extreme spin-up rate (G. Vasilopoulos et al. 2018) and the ∼0.25c outflow (P. Kosec et al. 2018) further confirm that the X-ray emission is powered by accretion on to a compact object rather than, for example, colliding wind shocks.

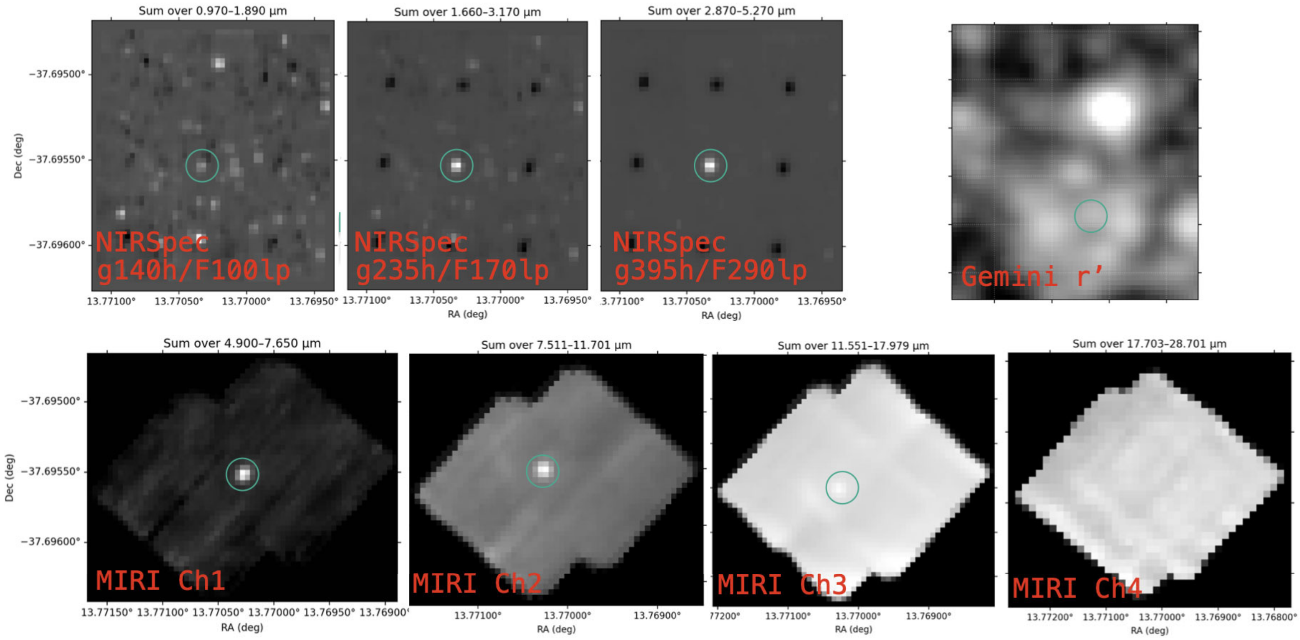


**Figure 1.** Collapsed IFU cubes for NIRSpec and MIRI. The location of the source is indicated with a circle. In the top right, we show a Gemini $r'$ band image taken in 2024 November (A.-N. Chené et al. 2025).

## 2 OBSERVATIONS AND DATA

### 2.1 VLT

NGC 300 ULX-1 was re-observed with the VLT X-Shooter instrument on 2023 October 25 as part of programme ID 0109.D-0813 (PI: Heida). The data consist of a near-infrared spectrum covering 0.58–2.48 µm at a resolving power of $R \approx 11\,400$, with a total exposure time of 3000 s.

### 2.2 *JWST*

Spectra of ULX-1 were taken as part of *JWST* Cycle 2 programme 3738 (PI: Beasor) on 2024 November 11. Observations were taken using the Mid-Infrared-Instrument (MIRI) in medium resolution spectroscopy (MRS) mode and the Near-Infrared Spectrograph (NIRSpec) in IFU mode.

The NIRSpec IFU provides a 3 arcsec × 3 arcsec field of view with spatial sampling of 0.1 arcsec per spaxel and enables simultaneous spatially resolved spectroscopy across the 0.6–5.3 µm wavelength range. The grating/filters used were G140H/F100LP, G235H/F170LP, and G395H/F290LP, covering 0.97–5.27 µm. The total on-source integration time was 5835.552 s. The target was centred in the IFU field using the standard NIRSpec target acquisition procedure. Observations were obtained using a four-point nod dither pattern to improve spatial sampling and mitigate detector artefacts.

The MIRI MRS provides integral-field spectroscopy over the wavelength range 4.9–28.8 µm with a spectral resolving power of $R \sim 1500$–3500, depending on wavelength. The data were acquired in all four MRS channels, each comprising three sub-bands (A, B, C) to cover the full spectral range. The total on-source integration time was 2220.032 s. The target was centred in the MRS field of view using the dedicated target acquisition procedure. As for the NIRSpec observations, a four-point nod dither pattern was used.

The Level 3 data were retrieved from the Mikulski Archive for Space Telescopes (MAST[2]) and were reduced using the Calibration Reference Data System (CRDS) version 11.17.25. In both cases the spectra were extracted using JDAVIZ software. The source spectra were extracted using circular apertures encapsulating the visible flux summed across all wavelengths. In Fig. 1, we show the collapsed data cubes for each instrument and filter combination, as well as the location of the source compared to a recent Gemini $r'$ image (A.-N. Chené et al. 2025).

## 3 RESULTS

In Fig. 2, we show the 2022 X-Shooter spectrum alongside the the 2018 spectrum for comparison. The 2022 spectrum is fainter than the 2018 spectrum by a factor of 10 between 0.6 and 2.5 µm. We no longer see the absorption features characteristic of a cool, extended atmosphere (TiO, CO) that were present in the 2018 spectrum.

In Fig. 3, we show the extracted spectrum of ULX-1 including both *JWST* NIRSpec and MIRI data. The newly observed spectral energy distribution (SED) appears significantly redder than the 2018 X-Shooter observations of the RSG-like counterpart to ULX-1. Indeed, the flux at ∼1 µm is fainter than the RSG-like spectrum by a factor of 10. Between 1 and 8 µm, we find a cool, red component that can be approximately fit with a 900K blackbody spectrum.[3] Beyond that, the SED appears to have a broad hump at 10–14 µm. We note however that this feature is narrower than

[2] https://mast.stsci.edu/

[3] We note the absorption feature-like lines in the NIRSpec data are artefacts from the gap between CCDs.

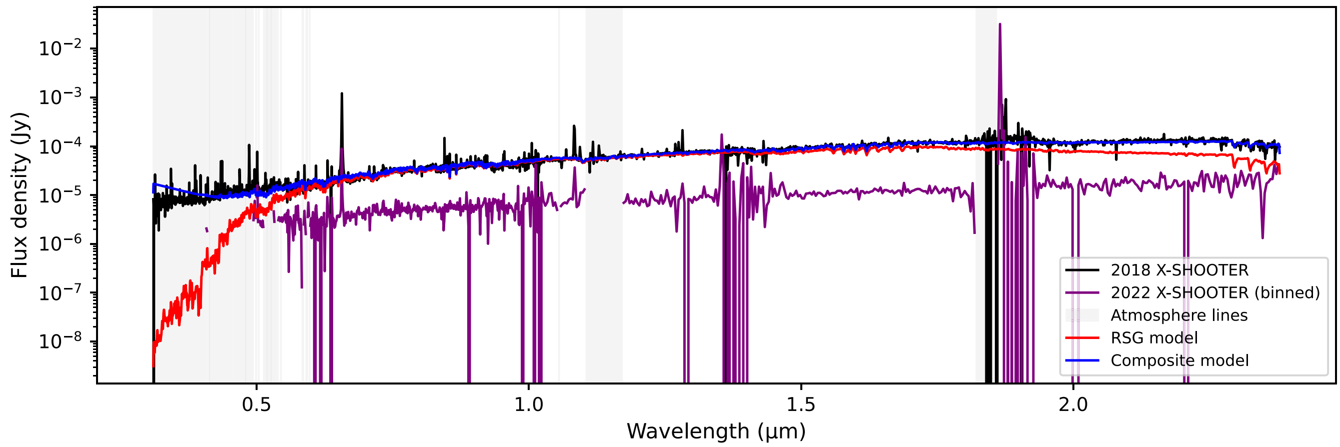


**Figure 2.** X-Shooter spectra of the donor star taken in 2018 (black line) and in 2022 (purple line), along with the best-fitting model to the 2018 spectrum presented in M. Heida et al. (2019) (red and blue lines). We mark the position of atmospheric absorption lines with grey bars. The 2022 spectrum has been binned to reduce noise.

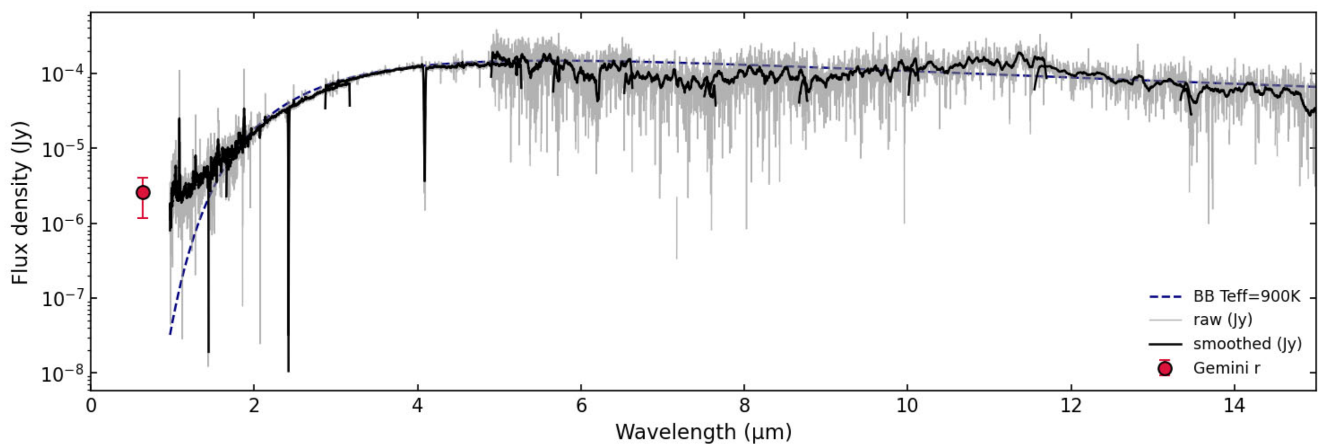


**Figure 3.** NIRSpec and MIRI spectra of ULX-1. We show the raw data (grey line) and smooth data (black line). The data have been smoothed using a moving average with a 50-pixel window for MIRI data and a 20-pizel window for NIRSpec data. We also overplot a 900 K blackbody spectrum (dashed blue line) and the Gemini r' photometry point (red point) from A.-N. Chené et al. (2025).

a blackbody, and it also peaks at too long of a wavelength to be silicate emission (which peaks at around 10 μm). In Fig. 3, we also show the Gemini $r'$ ($\lambda = 0.64\,\mu$m) photometry presented in (A.-N. Chené et al. 2025) with a red dot.

### 3.1 Luminosity

We now compare the luminosity of the observed infrared component to the luminosity of the RSG-like companion star reported by M. Heida et al. (2019). To do this, we integrate under the observed SED and assume a distance of 1.86 Mpc (J. J. Dalcanton et al. 2009), finding a luminosity of $\log(L/\mathrm{L}_\odot) = 4.10{\pm}0.01$. This is 56 per cent of the luminosity of the RSG-like source in 2018 (M. Heida et al. 2019), but is consistent with progenitor luminosity estimates from V. A. Villar et al. (2016) and R. M. Lau et al. (2016), see Section 3.3. We note that there is likely flux below our shortest wavelength point, and beyond our longest wavelength point. To compensate for this, we extrapolate the observed flux with a blackbody spectrum and include that in the luminosity calculation. For the blue flux, we extrapolate a 900 K blackbody between 0 and 0.97 μm. For the red flux, we extrapolate a 400 K blackbody between 17.98 and 1000 μm. We find that the missing flux contribution is 2.3 per cent, or 0.01 dex. To ensure the robustness of these assumptions, we also vary the two blackbody temperatures by ±200 K, finding this makes minimal difference on the derived luminosity. As such, our total luminosity is $\log(L/\mathrm{L}_\odot) = 4.11 \pm 0.02$.

### 3.2 Dust shell modelling

We model the observed SED using the radiative transfer code DUSTY (Z. Ivezic, M. Nenkova & M. Elitzur 1999). We assume the surviving central star is a cool supergiant (V. A. Villar et al. 2016) and explore a range of effective temperatures ($T_{\mathrm{eff}} = 2500$, 3900, 5000, 7000 K). We created a grid of dust shell models varying the inner dust temperature ($T_{\mathrm{in}}$), optical depth ($\tau_{\mathrm{V}}$), grain size ($a$), and grain composition, as summarized in Table 1.

The choice of grain composition strongly governs the shape of the mid-infrared SED. Pure silicate dust (Sil) produces a pronounced feature near ∼10 μm, while pure graphite (grf) and amorphous carbon (amC) yield smooth, featureless continua that fail to reproduce the broad emission evident in the observed SED

**Table 1.** Parameters of the DUSTY model grid. All models assume a spherically symmetric dust shell with a density profile $\rho \propto r^{-2}$ and an outer radius $Y = r_{out}/r_{in} = 10^4$. Optical depths $\tau_V$ are evaluated at $\lambda = 0.55$ µm. For SiC-Pg models, an extended grain size grid was also explored. Sil-DL and grf-DL are the silicate and graphite grains of B. Draine & H. M. Lee (1984), amC-Hn is amorphous carbon (M. S. Hanner 1988), SiC-Pg is silicon carbide (B. Pégourié 1988), and $Al_2O_3$ is alumina.

| Parameter | Range |
|---|---|
| $T_{eff}$ | 2500, 3400, 3900, 5000, 7000 K |
| $T_{in}$ | 400–1200 K, steps of 100 K |
| $T_{in}$ (SiC-Pg only) | 400–2000 K, steps of 100 K |
| $\tau_V$ | 1.0–15.0 (steps of 1.0) |
| $a$ | 0.01, 0.3, 0.5, 1.0 µm |
| $a$ (SiC-Pg only) | $10^{-4}$, $10^{-3}$, $10^{-2}$, 0.05, 0.1, 0.3 µm |
| Composition | Sil-DL : grf-DL = 100:0, 50:50 |
| | amC-Hn = 100 |
| | SiC-Pg = 100 |
| | $Al_2O_3$ = 100 |

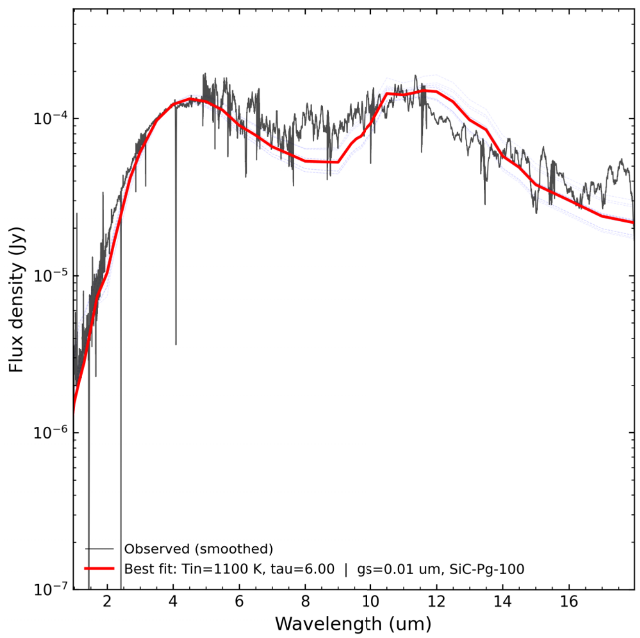


**Figure 4.** *JWST* NIRSpec and MIRI spectrum of SN 2010da/NGC 300 ULX-1 (black line) with the best-fitting DUSTY radiative transfer model overlaid (red line). The best-fitting model adopts SiC-Pg (silicon carbide) grains with $T_{eff} = 3400$ K, $T_{in} = 1100$ K, $\tau_V = 6.0$, and $a = 0.01$ µm. The dashed blue lines show all models within $\chi^2_{min} + 3\sigma$, illustrating the range of dust shell parameters consistent with the observed SED. The shape of the broad emission feature peaking near ∼11 µm is naturally reproduced by the SiC models, and is not reproduced by any other composition in our grid. The data have been smoothed using a moving average with a 50-pixel window for MIRI and a 20-pixel window for NIRSpec.

at ∼11 µm. Mixed silicate and graphite compositions (B. Draine & H. M. Lee 1984) suppress the silicate feature but do not produce emission at these wavelengths. Alumina ($Al_2O_3$) models similarly fail to reproduce the observed feature shape.

In contrast, models incorporating silicon carbide grains (SiC) naturally reproduce the shape of the broad emission feature peaking near ∼11 µm that is characteristic of the observed SED. In Fig. 4, we show our best-fitting DUSTY model, which adopts SiC

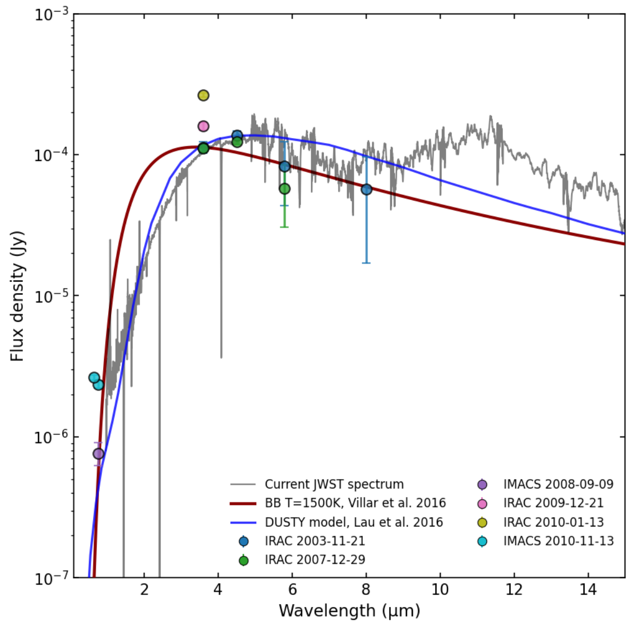


**Figure 5.** *JWST* spectrum with pre-outburst photometry overplotted. We also show the best-fitting blackbody ($T_{BB} = 1500$ K) from V. A. Villar et al. (2016) (red line) and the best-fitting DUSTY model from R. M. Lau et al. (2016) ($T_{eff} = 7000$ K, $T_{in} = 1000$ K, $\tau_V = 5$, blue line).

grains with $T_{eff} = 3400$ K, $T_{in} = 1100$ K, $\tau_V = 6.0$. The optical properties of the dust are described in B. Pégourié (1988). We find that the best-fitting grain size is $a = 0.01$ µm, smaller than the grains typically assumed for evolved star dust shells (typically between 0.3–3µm, S. Amari, R. S. Lewis & E. Anders 1994). Interestingly, the presence of SiC emission is typically associated with carbon-rich evolved stars, such as asymptotic giant branch stars (AGBs; e.g. B. Pégourié 1988; G. C. Sloan & others 2024; M. L. Boyer & others 2025). SiC grains are also among the most abundant presolar grains identified in meteorites, suggesting that carbon-rich stellar outflows may be a significant source of dust in the early Solar system (E. Zinner 2014; L. R. Nittler & F. Ciesla 2016).

### 3.3 Comparison to progenitor system

In Fig. 5, we plot the *JWST* spectra together with the progenitor photometry from *Spitzer*/IRAC and MMT/IMACS. The progenitor luminosity has previously been estimated by both V. A. Villar et al. (2016) and R. M. Lau et al. (2016), who found bolometric luminosities of $\log(L/L_\odot) = 4.28 \pm 0.06$ and $\log(L/L_\odot) = 4.18 \pm 0.06$, respectively. We note that R. M. Lau et al. (2016) adopted a distance of 2 Mpc to NGC 300. When updating this to 1.86 Mpc, their inferred luminosity is $\log(L/L_\odot) = 4.11 \pm 0.06$, consistent with the value reported in this work. In V. A. Villar et al. (2016), the luminosity was derived from a blackbody fit to the progenitor SED, yielding a temperature of ∼1500 K. R. M. Lau et al. (2016) modelled the progenitor photometry using radiative transfer calculations with DUSTY (Z. Ivezic et al. 1999), finding that the SED could be fit by a star embedded in a dusty circumstellar shell ($T_{in}$ = 1000 K, $\tau_V = 5$).

Importantly, in the progenitor SED a wide region around the peak of the blackbody was unconstrained because there was no photometry between <1 and 3.6 μm. With the continuous spectral coverage now available between 0.8 and 3.6 μm, we instead find the emission can be fit by a cooler temperature blackbody of ∼900 K (see Fig. 3). We note that the DUSTY model of R. M. Lau et al. (2016) closely matches the appearance of the *JWST* SED (see Fig. 5). Overall, the close match between the *JWST* spectrum and the R. M. Lau et al. (2016) model suggests that the luminous supergiant star has likely returned to its pre-outburst state, enshrouded by a cool dust shell.

## 4 DISCUSSION

We present new *JWST* NIRSpec and MIRI IFU observations of the peculiar system SN 2010da/NGC 300 ULX-1. These data reveal that the source has returned to a heavily reddened, infrared-dominated state, closely resembling its pre-2010 progenitor. The bolometric luminosity remains consistent with earlier estimates. The optical flux is strongly suppressed and the near- and mid-infrared emission dominates the SED.

Importantly, the current spectrum no longer exhibits the molecular absorption features (e.g. TiO, CO) that characterized the donor during its post-outburst phase when it resembled an RSG. Instead, the emission is well described by SiC dust reprocessing the luminosity of a deeply embedded central source. Together, these observations suggest that the RSG-like configuration observed between 2010 and 2018 did not represent the progenitor's long-term evolutionary state, but rather a transient phase following the 2010 outburst. The system has now returned to a dust-enshrouded configuration similar to that observed prior to the outburst.

Notably, the current SED is better characterized by the lower luminosity and carbon-rich dust chemistry more typical of an AGB star than an RSG, raising the question of whether the donor is in fact a C-rich AGB star whose RSG-like appearance was a temporary consequence of the outburst. In this picture, the enhanced luminosity during the post-outburst phase – driven by reprocessed NS accretion luminosity (see Section 4.1) – may have inflated the photosphere sufficiently to mimic the cooler effective temperature and molecular absorption features of an RSG.

### 4.1 A transient RSG phase induced by binary interaction

The pre-2010 progenitor of SN 2010da was already known to be highly obscured by circumstellar dust, with the majority of its luminosity emerging in the infrared (V. A. Villar et al. 2016). The appearance of a relatively unobscured RSG spectrum in the years following the 2010 transient therefore implies that the outburst temporarily altered the circumstellar environment and stellar structure of the donor.

We propose that the 2010 event disrupted or cleared the inner dusty envelope through a combination of radiative heating, shocks, and dynamical interaction, reducing the optical depth along the line of sight. Simultaneously, energy deposition into the outer stellar layers – likely associated with strong binary interaction – led to inflation of the donor's envelope, resulting in a cool, RSG-like atmosphere that we see in the 2018 X-Shooter spectrum (see Fig. 2). During this phase, the donor appeared optically bright and more luminous than the progenitor, and exhibited molecular absorption features characteristic of an extended, cool atmosphere.

### 4.2 Re-enshrouding and the return to a dusty state

The new *JWST* observations indicate that the system has since re-entered a dust-enshrouded phase, as it appeared before its 2010 eruption. The disappearance of molecular absorption features seen in the 2018 X-Shooter spectrum and the dominance of warm dust emission imply that circumstellar material has re-formed or re-condensed around the donor, once again obscuring the stellar photosphere.

For a temperature of ∼900 K and a luminosity of $\log(L/\mathrm{L}_\odot) = 4.1$, the characteristic radius of the emitting dust is of order $10^{14}$–$10^{15}$ cm. This scale is consistent with dust formation in a dense stellar wind or in recently ejected material that has cooled and become optically thick. The time-scale of several years between the optically bright RSG phase and the current obscured state could be explained by dust condensation and wind-driven mass-loss following the relaxation of the inflated stellar envelope. We therefore interpret the present appearance of ULX-1 as a return to the progenitor's original embedded state, rather than a new or terminal evolutionary phase.

We note that if the binary interaction responsible for the 2010 outburst is cyclical in nature, the pre-2010 dust-enshrouded state of the progenitor may not represent a quiescent stellar wind, but rather the remnant of a previous eruption episode. In this picture, the system undergoes repeated cycles of envelope disruption, a transient optically bright RSG-like phase, and subsequent re-enshrouding as newly formed dust obscures the donor.

### 4.3 An envelope interaction

The products of binary interactions are predicted to show considerable diversity in their evolutionary outcomes, including extended supergiant phases and altered mass-loss histories (e.g. D. Pauli et al. 2026). We speculate that the observed sequence of events in SN 2010da/ULX-1 can be explained by a brief interaction between the neutron star and the outer envelope of the donor star (see e.g. D. Shishkin & N. Soker 2020). In this scenario, the neutron star temporarily grazed or penetrated the donor's envelope during a periastron passage or an episode of unstable mass transfer, triggering the 2010 outburst. The associated energy injection inflated the envelope, enhanced mass-loss, and disrupted or destroyed the inner dusty environment. RSGs in this mass range are also susceptible to runaway radial pulsations in their late evolutionary stages, with surface velocities potentially exceeding the local escape velocity (S. Sengupta, D. Sujit & A. Sarangi 2025; A. Suzuki & T. Shigeyama 2025); such pulsation-driven instability may have compounded the effects of the binary interaction, further enhancing mass-loss and envelope inflation during this phase. For ULX-1, this led to a prolonged phase of elevated accretion on to the neutron star, thus elevating the X-ray luminosity between 2010 and 2018, as well as causing the appearance of a cool, luminous donor.

However, the interaction did not result in a full inspiral or a common-envelope phase. Instead, the system subsequently detached, the donor envelope contracted, and dust formation resumed, restoring the system to an embedded, pre-outburst-like configuration with declining accretion from 2018 onwards.

### 4.4 Implications for the failed SN scenario

A.-N. Chené et al. (2025) proposed that the donor star may have undergone a silent core collapse into a BH in 2019, producing

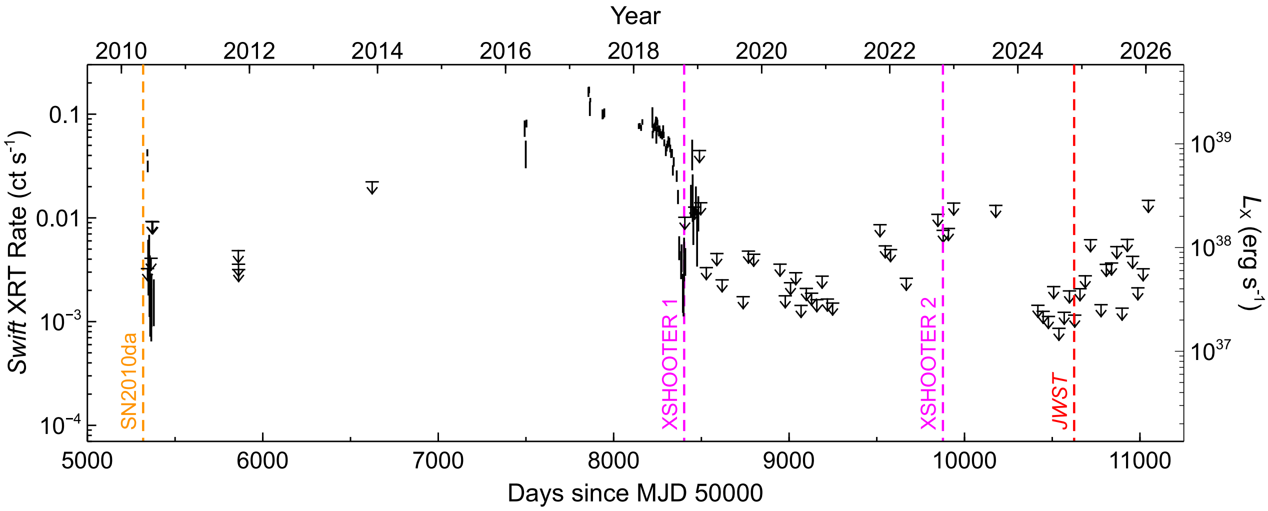


**Figure 6.** The X-ray lightcurve (0.3–10.0 keV) of ULX-1 from the *Neil Gehrels Swift Observatory* (*Swift*; N. Gehrels et al. 2004) following its 2010 outburst. The data have been extracted using the standard online XRT pipeline (P. A. Evans et al. 2009). During the main period of activity (prior to MJD 58500) the data are shown on a per-observation basis, while after this date we extract the XRT data using ~month-long bins to better showcase the limits on continued activity placed by *Swift*; where only upper limits on the brightness can be placed, these are computed at the 2$\sigma$ level. In addition to showing the evolution of the X-ray luminosity, we also indicate the date of the SN2010da event (that we take to mark the onset of the outburst) and the dates on which optical/IR spectra were taken with vertical dashed lines.

a 'failed SN'. This scenario was motivated by the abrupt decline in optical brightness between 2018–2024 and changes in the accretion regime. We note that models of failed SNe vary in their predictions regarding the expected amount of fading, time-scale, presence of IR emission, and X-ray emission (see discussion in E. R. Beasor et al. 2026), but in general a failed-SN outcome predicts: (1) a drastic drop in *bolometric* luminosity, (2) continued fading as accretion on to the nascent BH declines, and (3) no sustained IR output powered by a surviving stellar photosphere. ULX-1 stands in contrast to two other failed SN candidates, N6946-BH1 (S. M. Adams et al. 2017; E. R. Beasor et al. 2024) and M31-2014-DS1 (K. De et al. 2024; E. R. Beasor et al. 2026), which both appear to show a substantial drop in bolometric luminosity between the pre-disappearance and post-disappearance epochs. While the reason for this drop in luminosity is debated, given that ULX-1 has now returned to its pre-outburst luminosity and appearance, it would seem the system is in a different category the aforementioned failed SN candidates. For ULX-1, the failed SN scenario can be ruled out.

### 4.5 Proposed timeline

Taken together, the observations support an evolutionary scenario in which the donor alternated between a dust-enshrouded supergiant phase and a temporarily inflated, RSG-like configuration following episodes of strong binary interaction. We briefly outline a possible evolutionary sequence below:

(i) **Pre-2010:** A dust-enshrouded supergiant with infrared-dominated emission.

(ii) **2010 outburst:** Interaction between donor and NS clears inner dust and inflates the stellar envelope.

(iii) **2010–2018:** Transient RSG-like phase with reduced obscuration and elevated accretion, culminating in the ULX-level luminosities that define this system. This is supported by the increasing X-ray luminosity through this time (see Fig. 6).

(iv) **2018–present:** Re-enshrouding as dust reforms and the system returns to an embedded state, accompanied by a marked decline in accretion rate. The *Swift*/XRT monitoring demonstrates that ULX1 must have returned to at least sub-Eddington levels of accretion on average following this transition, even if a non-negligible level of accretion has persisted. The most recent firm X-ray detection – a *Chandra* observation in 2020 (MJD 58965) yielding $L_X \sim 10^{37}$ erg s$^{-1}$ (A.-N. Chené et al. 2025) – is consistent with all subsequent monthly XRT upper limits, meaning we cannot yet constrain whether the source has settled into a persistent low-luminosity state at this level or has faded further toward quiescence. Either way, both scenarios represent a substantial drop from the peak accretion rate responsible for the ULX-phase luminosities (see Fig. 6).

## 5 CONCLUSIONS

We have presented new *JWST* NIRSpec and MIRI IFU spectroscopy of SN 2010da/NGC 300 ULX–1, revealing that the system remains luminous but is now heavily obscured by warm, optically thick dust. The disappearance of molecular absorption features associated with the previously observed RSG-like spectrum, combined with only a modest decline in bolometric luminosity, strongly indicates that the donor star has survived and returned to its pre-2010 outburst state.

Our *JWST* observations rule out a failed supernova scenario, which would predict a far more dramatic and sustained decline in bolometric luminosity. Instead, the data point to a major, non-terminal event that temporarily triggered by interaction between the NS and the donor star, that altered the circumstellar environment and accretion state of the system. The rapid photometric and spectroscopic evolution observed over the past 16 yr underscores the importance of continued multiwavelength monitoring. Given that this is a binary system, we may expect further outbursts analogous to the 2010 event in the future, which would provide conclusive confirmation of this scenario. SN 2010da/ULX-1 may be analogous to the quasi-periodic SN impostors SN 2000ch (M. Aghakhanloo et al. 2023a) and AT 2016blu/NGC 4559ot (M. Aghakhanloo et al. 2023b), which exhibit recurrent eruptive behaviour driven by episodic mass-loss and circumstellar interaction, albeit on shorter time-scales likely set by their more compact progenitor systems.

## ACKNOWLEDGEMENTS

We would like to thank the anonymous referee whose comments helped improve the paper. The authors would like to thank Sebastian Kamann for useful discussions on working with IFU data and Kishalay De for providing NEOWISE lightcurves at the proposal stage. The authors would also like to thank André-Nicolas Chené for useful discussions. ERB is supported by a Royal Society Dorothy Hodgkin Fellowship (grant no. DHF-R1-241114). DJW acknowledges support from the Science and Technology Facilities Council (STFC; grant code ST/Y001060/1). This work is based on observations made with the NASA/ESA/CSA *JWST*. The data were obtained from the Mikulski Archive for Space Telescopes at the Space Telescope Science Institute, which is operated by the Association of Universities for Research in Astronomy, Inc., under NASA contract NAS 5–03127 for *JWST*. These observations are associated with programme 3738.

## DATA AVAILABILITY

The *VLT* X-Shooter spectra are available via the ESO Data Archive. The *JWST* data are available via MAST (doi:10.17909/p3m4-s245).

## REFERENCES

Abbott B. P. et al., 2017, Phys. Rev. Lett., 118, 221101
Adams S. M., Kochanek C. S., Gerke J. R., Stanek K. Z., Dai X., 2017, MNRAS, 468, 4968
Aghakhanloo M. et al., 2023a, MNRAS, 521, 1941
Aghakhanloo M. et al., 2023b, MNRAS, 526, 456
Amari S., Lewis R. S., Anders E., 1994, Geochim. Cosmochim. Acta, 58, 459
Bachetti M., Harrison F., Walton D. J., et al., 2014, Nature, 514, 202
Beasor E. R., Smith N., 2022, ApJ, 933, 41
Beasor E. R., Davies B., Smith N., van Loon J. T., Gehrz R. D., Figer D. F., 2020, MNRAS, 492, 5994
Beasor E. R., Hosseinzadeh G., Smith N., Davies B., Jencson J. E., Pearson J., Sand D. J., 2024, ApJ, 964, 171
Beasor E. R., Smith N., Pearson J., Subrayan B., Berger E., Sand D. J., Strader J., 2026, MNRAS, 546, 3
Binder B., Williams B. F., Kong A. K. H., Gaetz T. J., Plucinsky P. P., Dalcanton J. J., Weisz D. R., 2011, ApJ, 739, L51
Binder B., Williams B. F., Kong A. K. H., Gaetz T. J., Plucinsky P. P., Skillman E. D., Dolphin A., 2016, MNRAS, 457, 1636
Binder B. A., Carpano S., Heida M., Lau R., 2020, Galaxies, 8, 17
Boyer M. L. et al., 2025, ApJ, 991, 24
Caballero I., Wilms J., 2012, A&AR
Carpano S., Haberl F., Maitra C., Vasilopoulos G., 2018, MNRAS, 476, L45
Chené A.-N., Vasilopoulos G., Oskinova L. M., Martínez-Vázquez C., 2025, ApJ, 983, 53
Chornock R., Berger E., 2010, Astron. Telegram, 2637, 1
Dalcanton J. J. et al., 2009, ApJS, 183, 67
Davies B., Beasor E. R., 2020a, MNRAS, 493, 468
Davies B., Beasor E. R., 2020b, MNRAS, 496, L142
De K. et al., 2024, preprint (arXiv:2410.14778)
De Kishalay et al., 2026. Science, 391, 689
Draine B., Lee H. M., 1984, ApJ, 285, 89
Eksi K. Y., Andac I. C., Cikintoglu S., Gencali A. A., Gungor C., Oztekin F., 2015, MNRAS, 448, L40
Evans P. A. et al., 2009, MNRAS, 397, 1177
Farmer R., Renzo M., Götberg Y., Bellinger E., Justham S., de Mink S. E., 2023, MNRAS, 524, 1692
Fürst F. et al., 2023, A&A, 672, A140
Gehrels N. et al., 2004, ApJ, 611, 1005
Georgy C., 2012, A&A, 538, L8
Hanner M. S., 1988, ApJ, 334, L11
Heida M. et al., 2019, ApJ, 883, L34
Hirai R., Podsiadlowski P., 2022, MNRAS, 517, 4544
Israel G. L., Stella L., Bachetti F., et al., 2017, Science, 355, 817
Ivezic Z., Nenkova M., Elitzur M., 1999, Astrophysics Source Code Library, 1, 11001
Kaaret P., Feng H., Roberts T. P., 2017, ARA&A, 55, 303
Kosec P., Pinto C., Walton D. J., Fabian A. C., Bachetti M., Brightman M., Fürst F., Grefenstette B. W., 2018, MNRAS, 479, 3978
Lau R. M. et al., 2016, ApJ, 830, 142
Middleton M., Gúrpide A., Walton D. J., 2023, MNRAS, 519, 2224
Moe M., Di Stefano R., 2017, ApJS, 230, 15
Nittler L. R., Ciesla F., 2016, ARA&A, 54, 53
Pauli D. et al., 2026, A&A, 707, A11
Pégourié B., 1988, A&A, 194, 335
Pinto C., Walton D. J., 2023, preprint (arXiv:2302.00006)
Podsiadlowski P., Cannon R. C., Rees M. J., 1995, MNRAS, 274, 485
Sana H. et al., 2012, Science, 337, 444
Sengupta S., Sujit D., Sarangi A., 2025, preprint (arXiv:2510.27189)
Shishkin D., Soker N., 2020, MNRAS, 497, 855
Sloan G. C. et al., 2024, Galaxies, 12, 61
Smartt S., 2015, Publ. Astron. Soc. Aust., 32, e016
Smith N., 2014, ARA&A, 52, 487
Smith N., 2026, Encyclopedia of Astrophysics, Vol. 2. p. 508
Smith N., Hartigan P., 2006, ApJ, 638, 1045
Smith N., Gehrz R. D., Hinz P. M., Hoffmann W. F., Hora J. L., Mamajek E. E., Meyer M. R., 2003, AJ, 125, 1458
Smith N., Li W., Filippenko A. V., Chornock R., 2011a, MNRAS, 412, 1522
Smith N., Li W., Silverman J. M., Ganeshalingam M., Filippenko A. V., 2011b, MNRAS, 415, 773
Smith N. et al., 2018, MNRAS, 480, 1466
Suzuki A., Shigeyama T., 2025, MNRAS, 543, 3929
Thorne K. S., Żytkow A., 1975, ApJ, 199, L19
Thorne K. S., Żytkow A., 1977, ApJ, 212, 832
Vasilopoulos G., Haberl F., Carpano S., Maitra C., 2018, A&A, 620, L12
Villar V. A. et al., 2016, ApJ, 830, 11
Walton D. J. et al., 2018, ApJL, 857, L3
Zinner E., 2014, Presolar Grains, 2nd edn. Elsevier, Oxford, p. 181

This paper has been typeset from a TEX/LATEX file prepared by the author.